INVESTIGATION OF THE FREE TURBULENT SWIRL JET BEHIND THE AXIAL FAN

by

Novica Z. JANKOVIĆ*

Hydraulic Machinery and Energy Systems Department,
Faculty of Mechanical Engineering, University of Belgrade, Belgrade, Serbia

Original scientific paper
https://doi.org/10.2298/TSCI160417197J

Experimental investigation of the free turbulent swirl jet behind the axial fan, by use of the three-component laser Doppler anemometry is presented in this paper. Axial fan generates Rankine swirl. Measurements have been performed in five vertical measuring sections downstream for one rotation number 1500 rpm. Time averaged velocity components and their profile transformation downstream were investigated. Statistical moments of the second, third and fourth order have been calculated and presented. The highest turbulence levels are reached in the central zone, more precisely – shear layer zone and in the injection zone. Skewness and flatness factors differ from normal Gaussian distributions. Turbulence swirl flow anisotropy is investigated by applying invariant maps. Most of the obtained results are positioned in the region of the three-component isotropic turbulence and axisymmetric expansion.

Key words: *free jet, turbulent swirl, laser Doppler anemometry, axial fan*

Introduction

Free turbulent swirl jets occur in technical systems and they are used in combustion, as well in separation controls. They are also generated by the wings and turbomachines. In this paper is presented experimental investigation of the free turbulent swirl jet at the axial fan outlet. This is recognized as the installation and setup category A for fans in the international standard ISO 5801 [1]. Category A site installation means free inlet and free outlet, what is followed in the research presented in this paper.

An overview of the turbulent swirl flow jet experimental research is presented in papers [2-14]. It was shown in [2] that the entrainment rate and angle of spread for the swirling jet was nearly twice that of the non-swirling free jet. In paper [12] authors presented investigations of the turbulent swirl flow generated by vane swirler. Nowadays this case is studied also by CFD. Swirl flow through a suddenly expanding circular pipe is investigated in [13]. For this numerical study authors used different LES and DES models. Experimental investigations with hot-wire anemometry probes and CFD analysis turbulent flow at the exit of a high-speed axial ducted fan are presented in [14]. Study of jets with different initial swirl distributions given is in [15]. Two different swirl types with two different swirl numbers are compared with non-swirl flow on the same test rig. Miniature five-hole probe is used for

* Author's e-mail: njankovic@mas.bg.ac.rs

three-component velocity measurements. In [16] is presented an experimental study, by use of hot-wire anemometry, on the effects of swirl on the development of an axisymmetric turbulent mixing layer. In paper [17] are presented one-component LDA measurements of swirl flow generated by guide vanes placed at the nozzle exit in the horizontal plane.

Investigation of swirl flows and their characteristics is very important for technical practice as well as understanding their appearance in the nature. Significant number of papers analyzes free swirl jets, but only few of them investigate swirl jets generated by axial fan.

Experimental test rig and measurement system

Experimental test rig is presented in fig. 1. The swirl generator is a variable pitch axial fan with nine blades designed by Protić[†]. It is designed after the rW = const. law. The outer impeller diameter is $D_a = 0.399$ m. The dimensionless hub ratio is $D_i/D_a = 0.5$. The blade angle at impeller diameter was adjusted to $\beta_{Ra} = 30^o$. The profiled bell mouth inlet is at the test rig inlet and axial fan is in built in pipe with the inner diameter 0.4 m after the international standard ISO 5801, category A.

The fan rotation speed was regulated by a fully automated thyristor bridge with error up to ±0.5 rpm, originally designed and made by Stojiljković [3, 4]. In this paper are presented experimental results for fan rotational speed n = 1500 rpm.

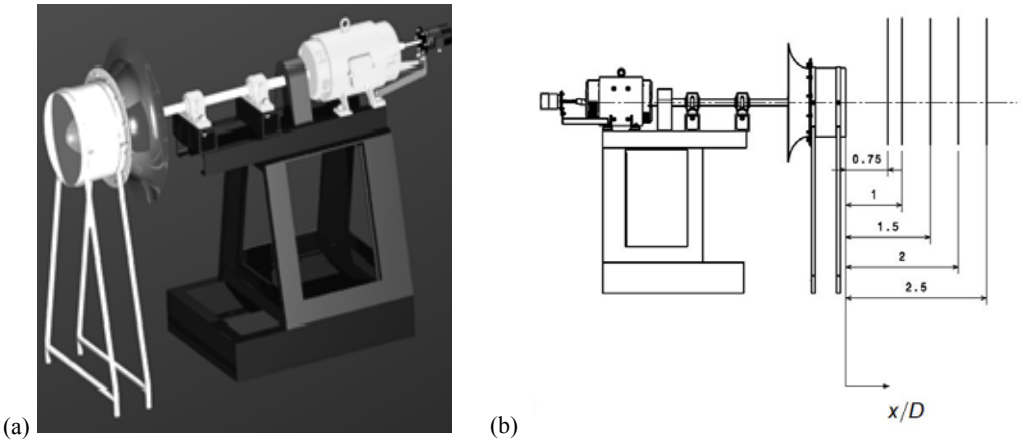

Figure 1. Test rig for experimental investigation; (a) main elements,(b) measuring sections

The measuring sections are presented in fig. 1(a) and denoted in tab. 1. The laser Doppler anemometry (LDA) has been employed along the vertical measuring sections at a 10 mm distance each. So, measurements have been performed in 76 measurements per each measuring section.

Table 1. Positions of the measuring sections

Measuring sections	I	II	III	IV	V
x/D	0.75	1	1.5	2	2.5

Three-components LDA by manufacturer TSI was used in these experiments. Continuum Ar-Ion laser of 5 W, by Coherent is used in these experiments. Two probes TSI

TR60 with beam expanders XPD60-750 used to form measurement volume. The TSI Flow Sizer software is used for acquisition and preliminary data analysis. The probes connected to photodetector module (PDM) by receiving fiber. The measurement focus with attached optics was on 757.7 mm. Laser wavelengths were 514.5 nm, 488 nm and 476.5 nm. The measurement volume diameter was app. 70 μm, while measurement volume length was app. 280 μm. Both LDA probes work in back scatter mode. The velocity was measured with uncertainty lower than 0.1%. Recording time of 20 s was set up as the stop criterion for all measurements. Laser power was 916 mW. Data frequency varied along the measuring sections. Measurements have been performed in the software coincidence mode and the highest sampling rate was 3.5 kHz, while most of the measurements had approximately 1.5 kHz.

The data acquisition was performed by use of the TSI software Flow sizer. Turbulence statistics is calculated by the in house code. The flow was seeded by the Antari Z3000II fog machine with liquid EFOG, Density Fluid, Invision [3]. It was naturally sucked in the test rig by the fan.

Experimental result and analysis

Integral characteristics

The distributions of all three velocities, in non-dimensional form, in all five measuring sections are presented in fig. 2, where U_m is averaged velocity by area. It is calculated on the basis of the mean axial velocity profile in the measuring section I and area $r/R = 1$. Reynolds number is $\mathrm{Re} = U_m D/\nu = 3.38 \cdot 10^5$.

The angle $\varphi = 90^o$ denotes the upper part (above-test rig axis) of the vertical diameter, while $\varphi = 270^o$ the lower part (under-test rig axis). It is obvious that more measurement points are obtained in the upper part. The smallest values for axial, circumferential, and consequently total velocities in the injection zone are reached for higher values of radius downstream. They are all in the interval from 1.4 to 2.2.

The Rankine vortex structures, as well as flow axisymmetry, are obvious in fig. 2. The minimum of axial velocity, fig. 2(a), and zero value of circumferential are reached in the same point – test rig axis ($r/R = 0$), *i. e.* in the swirl core for all measuring sections. The reverse flow occurs only in measuring sections I and II. The vortex core or *solid body* region is detected with almost linear increase of the circumferential velocity up to $r/R = 0.35$ for measuring sections I to IV, while for the measuring section V this zone is smaller, up to $r/R = 0.25$, fig.2(c). The maximum axial and circumferential velocities reach the highest values in the first measuring section, while they decrease downstream. In the free jet turbulent swirl flow axial velocity reach higher values than circumferential, what is not case in the conduit turbulent swirl flow [3-8]. The circumferential velocity maximum decreases for almost 45% downstream from the first measuring section to the last one, while axial around 30%. Circumferential velocity profiles, fig. 2(c), reveal vortex core region enlargement downstream. Mean radial velocity has the highest values in the vortex core region for the first measuring section, while in other measuring sections are reached even higher values (the absolute value) in the sound flow region. It has no high values, but its character discovers vortex core dynamics.

Average circulation obtained in the first measuring section has value $\Gamma = 5.41$ m^2/s, while swirl flow parameter is $\Omega = Q/(R\Gamma) = 1.53$. Swirl flow parameter is calculated as follows:

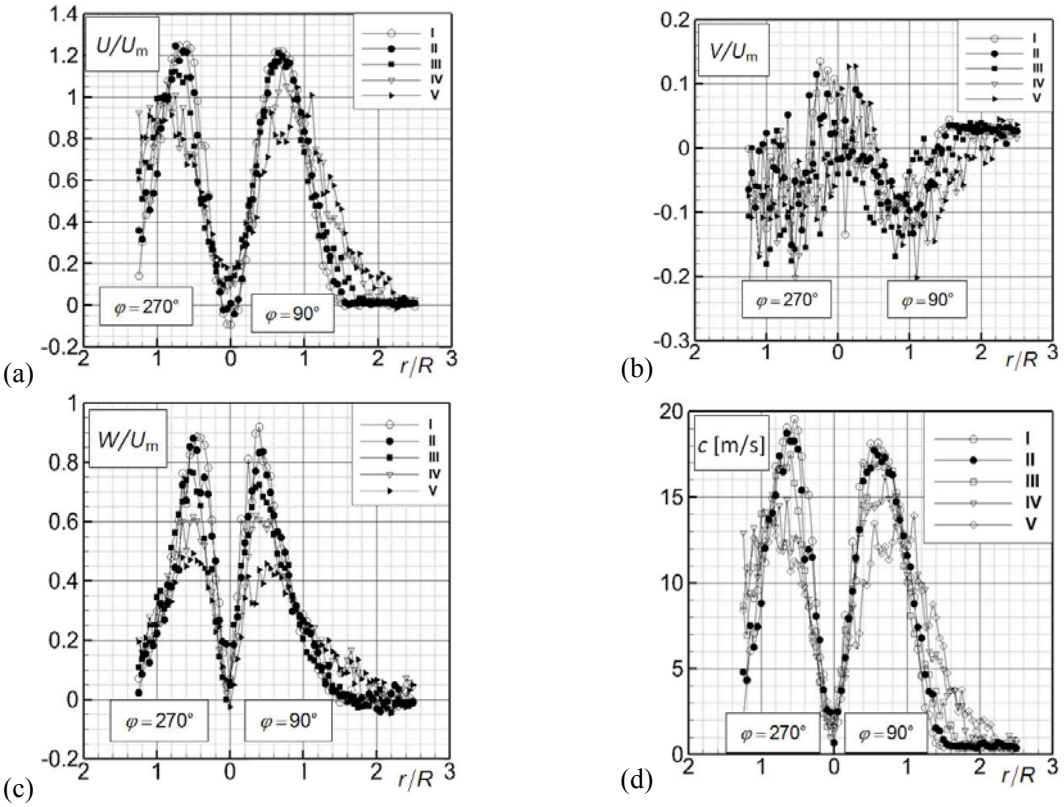

Figure 2. Distributions of the time averaged velocities in all five measuring sections in non-dimensional form; (a) axial (U), (b) radial (V), (c) circumferential (W), and (d) total velocity magnitude (c)

$$\Omega_i = \frac{Q_i}{R_i \overline{\Gamma}_i} = \frac{\left(\int_0^{R_i} rU\mathrm{d}r \right)^2}{R_i \int_0^{R_i} r^2 UW\mathrm{d}r} \tag{1}$$

where R = 0.2 m. It is obvious that the actual interest of this research is the complex high swirl intensity turbulent swirl jet where reverse flow exists. This is presented in fig. 2(a).

Turbulence statistics

Reynolds normal stresses, fig. 3, are calculated as:

$$\overline{u_i^2} = \sum_{j=0}^{N-1} \left(u_i^2 \right)_j \tag{2}$$

where the $u_i = u, v, w$ [3]. Turbulence intensity is calculated in the following way:

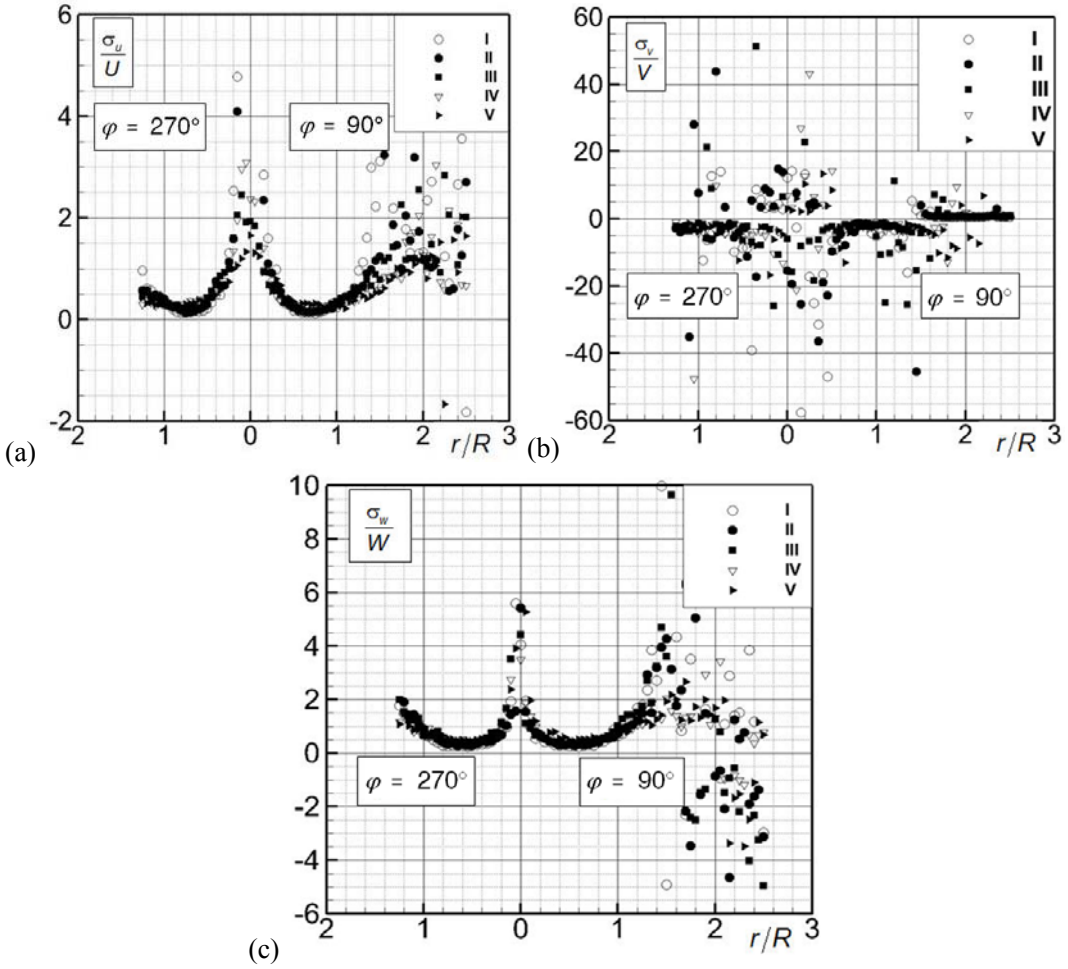

Figure 3. Turbulence levels in all five measuring sections for fluctuating velocities; (a) axial, (b) radial, and (c) circumferential

$$\frac{\sigma_i}{U_i} = \frac{\sqrt{\overline{u_i^2}}}{U_i} \tag{3}$$

It is noticeable that turbulence levels distributions are symmetrical for axial and circumferential fluctuating velocities and have the same character for all five measuring sections. The highest values are reached in the vortex core zones and injection zone which is more obvious for $\varphi = 90°$. The highest turbulence levels are reached for the radial velocity. Dimensionless normal stresses for all three velocities in the first, third and fifth measuring sections, are presented in fig. 4.

It is obvious that normal stresses decrease downstream. Character is the same in all measuring sections. In all cases maxima are reached for radial velocity, while the minima for circumferential. Anisotropy and non-homogeneity is dominant in the vortex core and shear layer regions. Anisotropy is weaker in the sound flow and injection regions.

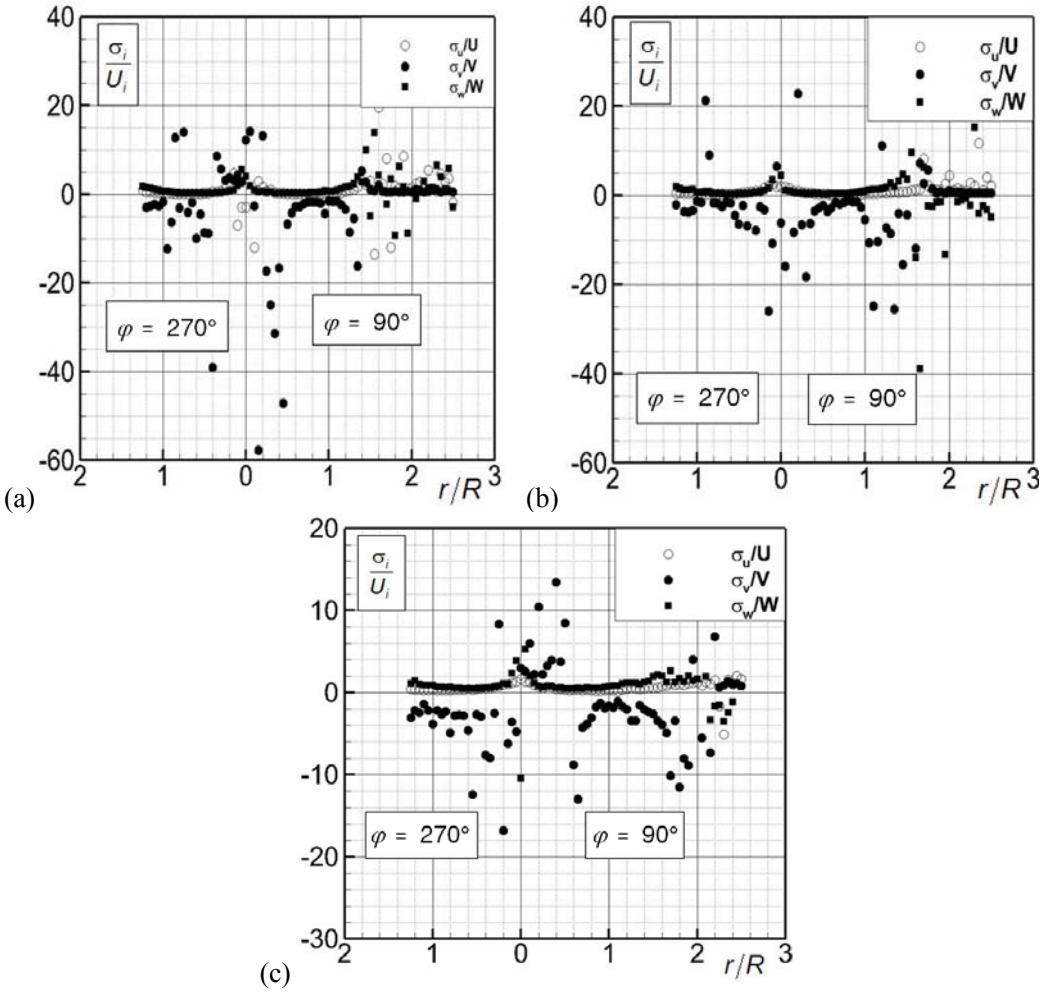

Figure 4. Distributions of the non-dimensional normal stresses in the measuring sections; (a) first, (b) third, and (c) fifth

The values of the normalized central moments for all three velocity components of the third S_i (skewness), and the fourth order F_i (flatness), where $u_i = u,v,w$, are calculated as:

$$S_i = \overline{u_i^3} / \sigma_i^3 , \; F_{u_i} = \overline{u_i^4} / \sigma_i^4 \tag{4}$$

Skewness factors for all three velocities in the first, third and fifth measuring sections are presented in fig. 5.

It is obvious that the largest deviation from the values for normal distribution ($S_i = 0$) is in the injection zone for all measuring sections. Negative skewness factors ($S_i < 0$) indicate that large velocity fluctuations are negative. This is obvious for axial velocity in sound flow region and for circumferential in the vortex core and shear layer regions dominantly for the first measuring section. Skewness factor for radial velocity has dominantly negative values and reach minima in the injection zone.

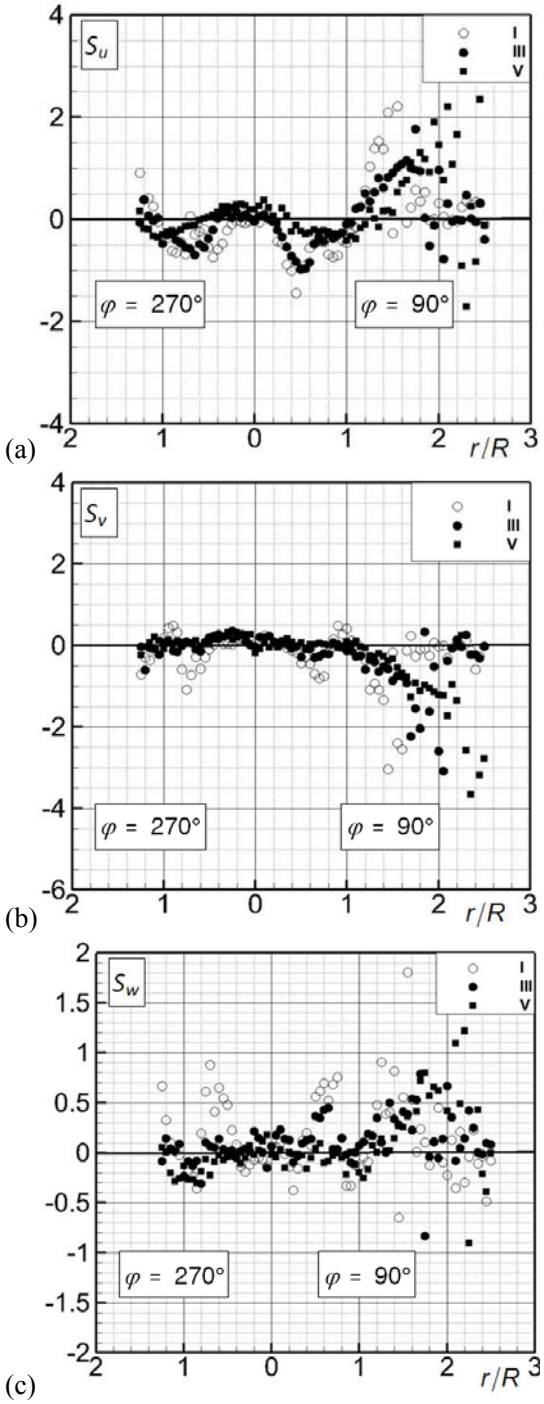

Figure 5. Skewness factors in the I, III and V measuring sections for velocities; (a) axial, (b) radial, and (c) circumferential.

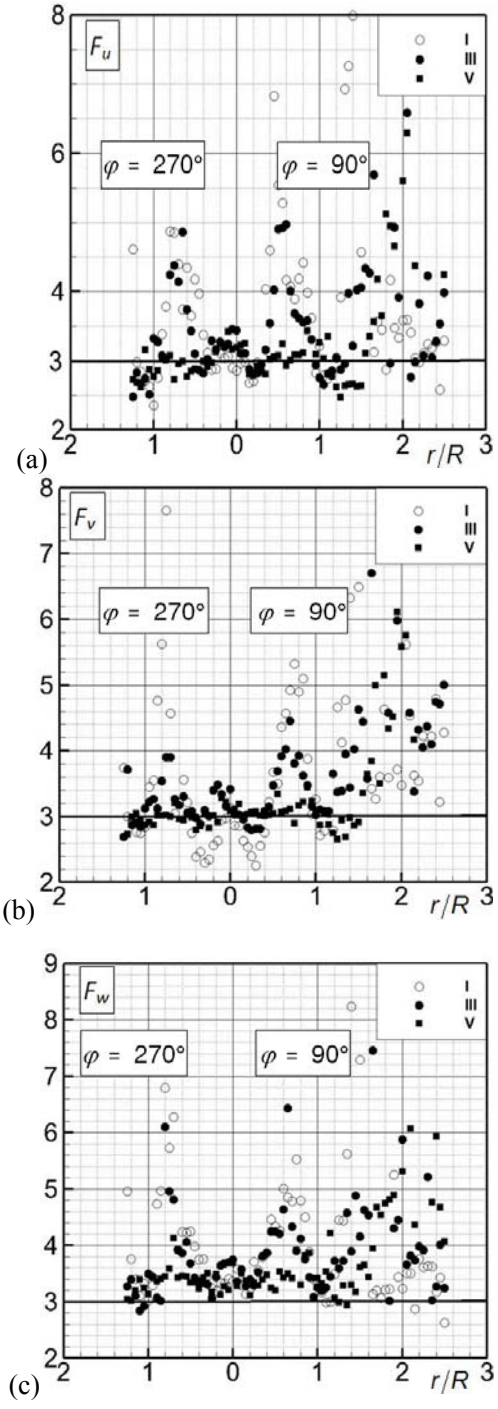

Figure 6. Flatness factors in the I, III and V measuring sections for velocities; (a) axial, (b) radial, and (c) circumferential

It is obvious that also flatness factors differ from the value for normal distribution (F_i = 3). Values greater than 3 (F_i > 3) indicate great probability of small fluctuations. This is a case for almost all values and measuring sections for circumferential velocity. These values are also dominant for other two velocities, fig. 6.

Radial distributions of the correlation moments, *i. e.* Reynolds shear stresses in the first, third and fifth measuring sections are presented in the normalized form in figs. 7(a)-7(c). These distributions characterize strong interaction between average and fluctuating velocity fields [4, 5].

Obtained Reynolds shear stresses ($-\rho\overline{uv}$, $-\rho\overline{uw}$, and $-\rho\overline{vw}$) are characteristic for turbulent swirl flow [3, 4]. Mean circumferential velocity has a dominant influence, not only on the formation of the vortex core and shear layer regions, but also on the turbulent transfer processes. Namely, stabilizing effect of the centrifugal force on turbulence depends on the angular velocity (W/r) distribution and sign of its partial derivative in the radial direction ($\partial r(W/r)$) [4, 5]. Reynolds shear stress has almost the same character in all three presented measuring sections, fig. 7(a). It has zero value at the test rig axis, maxima in the shear layer region. This moment reach minimum value in the first two specified measuring sections in point r/R = 1, while it is moved outwards (in the injection zone) for the last, fifth measuring section.

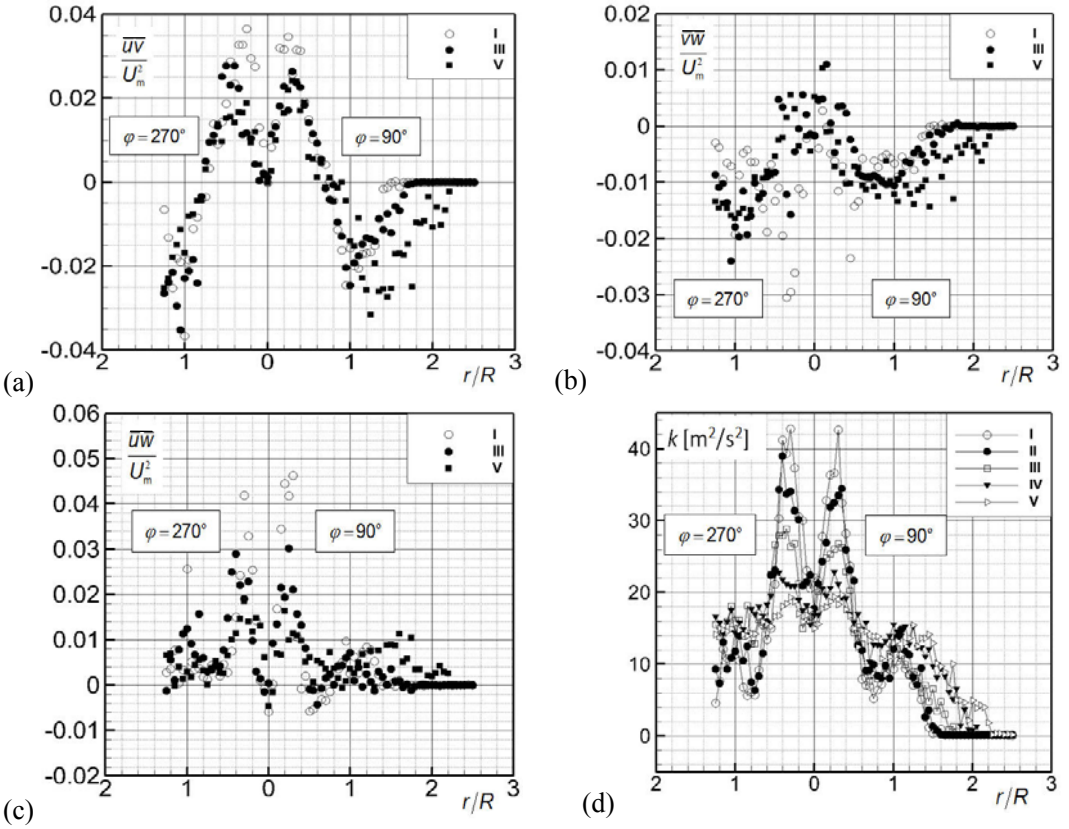

Figure 7. (a)-(c) Distributions of normalized correlation moments in three measuring sections and (d) distribution of the turbulence kinetic energy for all five measuring sections

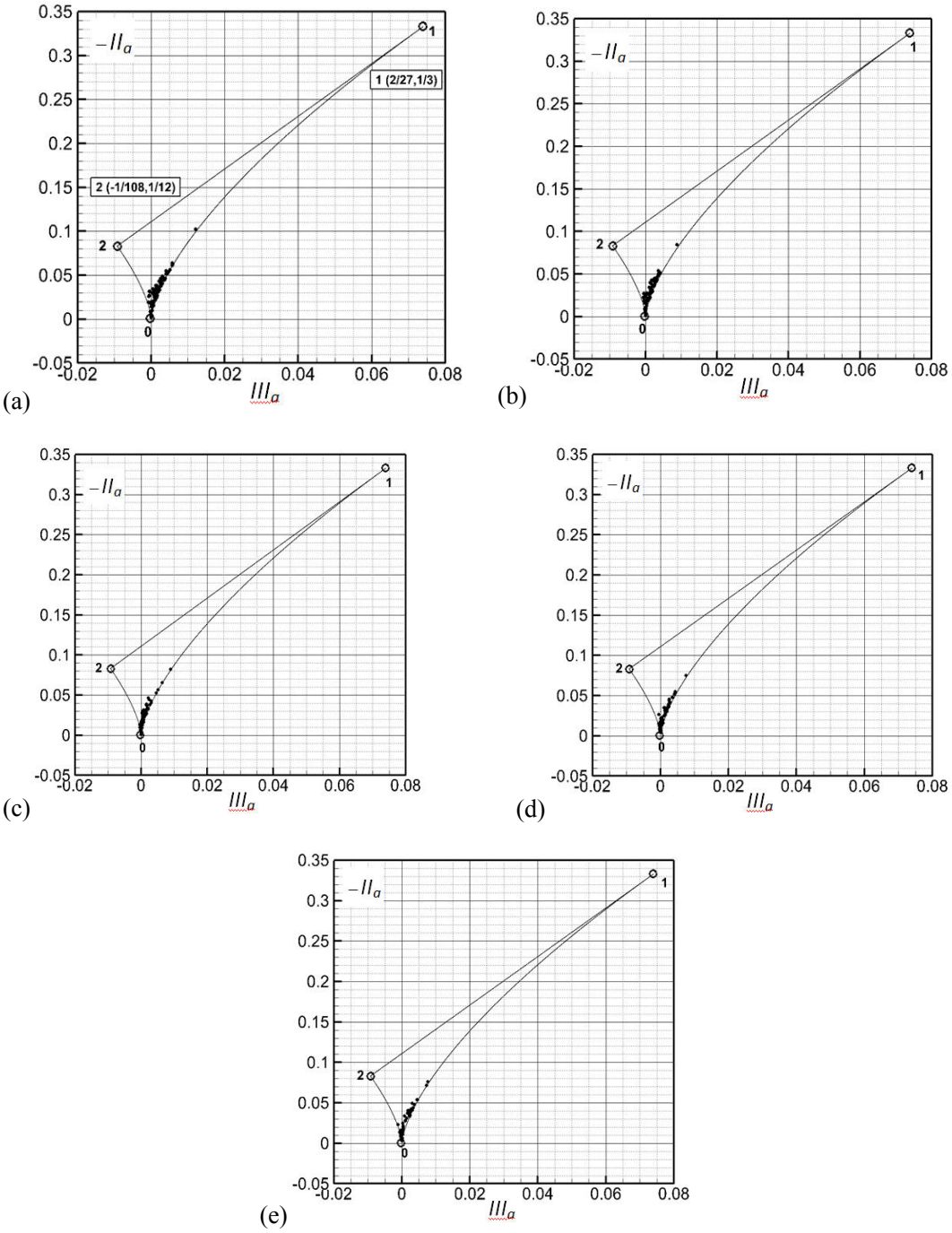

Figure 8. Invariant maps for the measuring sections I to V, respectively

It is obvious that Reynolds shear stresses ($-\rho\overline{uv}$ and $-\rho\overline{vw}$) have obvious increase in the injection zone, what is not so obvious, but exists in some parts for the third Reynolds shear stress also.

This seems to be promising regarding the mixing processes in this flow region.

Turbulent kinetic energy k is calculated in the following way:

$$k = \frac{1}{2}\left(\overline{u^2} + \overline{v^2} + \overline{w^2}\right) \tag{5}$$

Turbulent kinetic energy radial distributions in all five measuring sections are presented in fig. 7(d). The highest values are reached in the vortex core region and have the same character in all measuring sections. Turbulence kinetic energy decreases downstream in the vortex core and shear layer regions, while it is opposite in other fluid flow regions.

Turbulence structure in the light of the invariant theory

Anisotropy tensor, with its components a_{ij}, was introduced as the measure of anisotropy [10]. Three independent invariants are defined as:

$$I_a = 0 \quad II_a = -\frac{1}{2}a_{ij}a_{ji} \quad III_a = \frac{1}{3}a_{ij}a_{ik}a_{jk} \tag{6}$$

where $a_{ij} = 1/(2k)\overline{u_i u_j} - 1/3\,\delta_{ij}$ and $k = 1/2(\overline{u^2} + \overline{v^2} + \overline{w^2})$, and where δ_{ij} is the Kronecker delta [3, 8, 9]. All possible states of turbulence anisotropy belong to the inner area bounded with curvilinear triangle 201, known also as Lumley triangle or Invariant map of anisotropy or simply invariant map, in coordinate system (III_a, $-II_a$). Invariant maps for all points in all presented measuring sections are shown in fig. 8. Coordinates of these characteristic points (0, 1 and 2), which describe boundary turbulence states, are given in fig. 8(a). Triangle vertex 0 describes three-component isotropic turbulence, while point 1 corresponds to the boundary layer of one-component isotropic turbulence and vertex 2 to two-component isotropic turbulence. Curve 201 describes states of axisymmetric turbulence, where curve 02 (with $III_a < 0$) denotes axisymmetric contraction and curve 01 (with $III_a > 0$) describes axisymmetric expansion. Line 21 describes two-component turbulence.

In presented invariant maps, most of the points are located in the lower part of the curve 01 and in the vicinity of the point 0. It is almost the same case for all measuring sections. Majority of the points in the vortex core region are located the vicinity of the point 0, what corresponds to the three-component isotropic turbulence and has good agreement with previous analysis in this paper. The other points asymptotically approach axisymmetric expansion, *i. e.* curve 01.

Conclusions

Experimental investigation of the turbulent swirl jet deals with the jet entering stagnant surroundings from the axial fan. Fan is a turbulent swirl generator and is installed after the international standard ISO 5801, category A – free inlet and free outlet. The actual interest of this research is a complex high swirl intensity free jet. Downstream transformations of the mean velocity profiles and turbulent statistical properties are studied. In addition invariant maps are calculated for all five measuring sections.

The Rankine vortex axisymmetric structure is detected at the axial fan outlet, *i. e.* at the first measuring section and the flow kept this character downstream. Circumferential velocity maxima are significantly lower downstream than axial, while injection zone is increased. It was also shown that vortex core region is increased downstream.

Turbulence statistics with the help of invariant maps proved non-homogeneity and various forms of anisotropy of the studied flow. Turbulence levels for axial and circumferential velocity are the highest in the vortex core and mixing layer regions. Skewness and flatness factors differ from normal distribution values in almost all points. Experimentally obtained Reynolds shear stresses reach maxima in vortex shear layer region and they have obvious increase in the injection zone. It was also shown that all the measurement points were located in lower part of the curve which represented turbulent states of the axisymmetric expansion.

It is planned, in further study, to reveal the shape of the injection, *i. e.* mixing zone, with the change of the swirl flow intensity.

Acknowledgment

Axial fan applied in this research is designed and constructed by Prof. Dr.-Ing. Zoran D. Protić†(1922-2010). Prof. Dr Zoran Stojiljković, designed and built a very precise original fan rotation speed regulator. This work was funded by the grant from the Ministry of Education, Science and Technological Development, Republic of Serbia (TR 35046), which is gratefully acknowledged.

Nomenclature

c – total velocity, [ms^{-1}]
D – inner pipe diameter, [m]
D_i – hub diameter, [m]
D_a – impeller diameter, [m]
F – flatness factor, [–]
n – fan shaft rotational speed, [rpm]
Q – volumetric flow rate, [m^{3}s^{-1}]
R – inner pipe radius, [m]
Re – Reynolds number (= $\rho vc/\mu$), [–]
r – radial coordinate, [m]
S – skewness factor, [–]
U – mean axial velocity, [ms^{-1}]
V – mean radial velocity, [ms^{-1}]
W – mean circumferential velocity, [ms^{-1}]
u – fluctuating axial velocity, [ms^{-1}]
v – fluctuating radial velocity, [ms^{-1}]
w – fluctuating circumf. velocity, [ms^{-1}]
x – axial coordinate along a pipe axis, [m]

Greek symbols

β_{Ra} – blade angle at impeller outlet diameter, [°]
Γ – average circulation, [m^{2}s^{-1}]
θ – swirl flow intensity, [–]
ν – kinematic viscosity, [m^{2}s^{-1}]
σ – root-mean-square of turbulent velocity fluctuations, [ms^{-1}]
φ – coordinate of the polar cylindrical coordinate system (x,r,φ), [°]
Ω – swirl flow parameter, [–]

References

[1] International Standard ISO 5801:2017: Fans – Performance Testing Using Standardized Airways.
[2] Pratte, B. D., Keffer, J. F., The Swirling Turbulent Jet, *J. of Basic Eng., 94* (1972), 4, pp. 739-747
[3] Čantrak, Đ., *et. al.,* Turbulent Swirl Flow Characteristics and Vortex Core Dynamics Behind Axial Fan in a Circular Pipe, *Proceedings*, CMFF'12, Budapest University of Technology and Economy, Budapest, Hungary, 2012, Vol. II, pp. 749-756
[4] Čantrak, Đ. S., Analysis of the Vortex Core and Turbulence Structure Behind Axial Fans in a Straight Pipe Using PIV, LDA and HWA Methods (in Serbian), Ph. D. thesis, University of Belgrade, Faculty of Mechanical Engineering, Belgrade, 2012
[5] Čantrak, S., Experimental Investigations of Statistical Properties of Turbulent Swirling Flows in Pipes and Diffusers (in German), Ph. D. thesis, University Karlsruhe, Karlsruhe, Germany, 1981

[6] Benišek, M. H. *et al.*, Investigation of the Turbulent Swirl Flows in a Conical Diffuser, *Thermal Science*, *14* (2010), Suppl., pp. S141 - S154
[7] Čantrak, Đ. S., *et al*., Investigation of the Turbulent Swirl Flow in Pipe Generated by Axial Fans using PIV and LDA Methods, *Theoretical and Applied Mechanics*, *42* (2015), 3, pp. 211-222
[8] Čantrak, Đ. S., *et. al.,* Laser Insight into the Turbulent Swirl Flow behind the Axial Flow Fan, *Proceedings*, ASME Turbo ASME TURBO EXPO 2014, Expo 2014: Turbine Technical Conference and Exposition, GT 2014, Technical track: Fans and Blowers, Dusseldorf, Germany, 2014, paper ID GT2014-26563
[9] Lumley, J. L., Newman, G., The Return to Isotropy of Homogeneous Turbulence, *Journal of Fluid Mechanics*, *82* (1977), Aug., pp. 161-178
[10] Elsner J. W., Drobniak S., Turbulence Structure in Swirling Jets, in: *Structure of Complex Turbulent Shear Flow*, *Proceedings*, IUTAM Symposium, Springer, Marseille, France, 1982, pp. 219-228
[11] Ilić, D. B., Swirl Flow in Conical Diffusers (in Serbian), Ph. D. thesis, Faculty of Mechanical Engineering, University of Belgrade, Belgrade, 2013
[12] Sander, G. F., Lilley, D. G., The Performance of an Annular Vane Swirler, *Proceedings*, Joint Propulsion Conference, Seattle , Washington D. C., USA, 1983, AIM paper No. 83-1326
[13] Javadi, A., Nilsson., H., LES and DES of Strongly Swirling Turbulent Flow through a Suddenly Expanding Circular Pipe, *Computers & Fluids*, *107* (2014), pp. 301-313
[14] Šekularac, M., Analysis of Flow Fields in Complex Ventilation Systems of Traffic Tunnels, Ph. D. thesis, Faculty of Mechanical Engineering, University of Montenegro, Podgorica, Montenegro, 2015
[15] Gilchrist, R. T., Naughton, J. W., Experimental Study of Incompressible Jets with Different Initial Swirl Distributions: Mean Results, *AIAA Journal*, *43* (2005), 4, pp. 741-751
[16] Mehta, R. D., *et al*., Some Effects of Swirl on Turbulent Mixing Layer Development, *Physics of Fluids*, *3* (1991), 11, pp. 2716-2724
[17] Sislian, J. P., Cusworth, R. A., Measurements of Mean Velocity and Turbulent Intensities in a Free Isothermal Swirling Jet, *AIAA Journal*, *24* (1986), 2, pp. 303-309

Paper submitted: April 17, 2016
Paper revised: June 25, 2016
Paper accepted: July 27, 2016

© 2017 Society of Thermal Engineers of Serbia.
Published by the Vinča Institute of Nuclear Sciences, Belgrade, Serbia.
This is an open access article distributed under the CC BY-NC-ND 4.0 terms and conditions.